Two-Body Models for Analyzing Complex Impedance [1]

Douglas A. Bennett, Robert D. Horansky and Joel N. Ullom

National Institute of Standards and Technology, 325 Broadway, Boulder, CO USA 80305-3328

Abstract. Complex impedance is an important and widely used technique for characterizing microbolometers and microcalorimeters. Often, complex impedance data from actual devices does not fit the simple one-body model of a TES microcalorimeter. In this paper we will review the range of possible two-body impedance models and compare them to our most recent measurements of microcalorimeters designed for gamma-ray spectroscopy. When possible, we indicate differences between models that may be used to identify the model that best describes a particular device.

Keywords: Microcalorimeters, Transition Edge Sensors, Impedance
PACS: 85.25.Oj, 85.25.Am, 07.20.Fw, 29.30.Kv

INTRODUCTION

Microcalorimeters using Transition Edge Sensors (TES) are being used in a growing number of applications that span an increasing variety of energy ranges. As instruments using these devices are being developed and deployed, the need for accurate modeling and characterization of TES devices becomes increasingly important. The trends towards larger arrays and practical applications require optimizations that are critically dependent on understanding the behavior of specific TES designs.

One widely used technique for characterizing microcalorimeters and bolometers that use a temperature dependent resistance is the measurement of the complex impedance where the response of the thermistor is measured as a function of the frequency of a signal applied to the thermistor bias [1, 2]. These measurements are widely used to determine thermal and electronic parameters in microcalorimeters and bolometers [3, 4, 5, 6]. Many complex impedance measurements can not be accurately fit by the simple one-body model usually associated with a TES [7]. When fitting the data, one is usually forced to use more complicated thermal models [2] in order to achieve a reasonable fit. Recent measurements of anomalously high heat capacity values for the common membrane material SiN provide new physical motivation for multi-body impedance models [8]. In an effort to optimize our arrays of γ-ray microcalorimeters, we are working on characterization and modeling techniques. In this paper we review the range of possible two-body impedance models and compare them to our most recent measurements of microcalorimeters designed for gamma-ray spectroscopy.

[1] Contribution of a U.S. government agency, not subject to copyright.

MODELING IMPEDANCE OF A TES

The simplest model of a voltage biased TES consists of heat capacity C_{TES} weakly coupled by a thermal conductance G to a heat sink at temperature T_b. The resistance of the TES (R_{TES}) is a function of both the temperature of the TES (T) and the electrical current (I). The TES is placed in parallel with a shunt resistance R_{sh} such that R_{TES} is larger then R_{sh} providing the TES with an approximate voltage bias. The Thevenin equivalent electrical circuit consists of a Thevinin-equivalent load resistance R_L in series with the steady state TES resistance R_0 and inductance L. The dynamics of this device describing the change in current and temperature with time in the small signal limit are described in the literature [7], defining $\mathscr{L}_I = P_{J0}\alpha_I/GT_0$, $P_{J0} = I_0^2 R_0$, $\alpha_I \equiv T_0/R_0\,(\delta R/\delta T)\,|_{I_0}$ and $\beta_I \equiv I_0/R_0\,(\delta R/\delta I)\,|_{T_0}$. The resulting circuit impedance can easily be calculated using Z matrix methods [1, 7] giving

$$\delta Z = \delta V/\delta I = R_L + i\omega L + Z_T \qquad (1)$$

where

$$Z_T(\omega) = R_0\,(1+\beta_I) + \frac{R_0\mathscr{L}_I}{1-\mathscr{L}_I}\frac{2+\beta_I}{1+i\omega\tau_I} \qquad (2)$$

with $\tau_I = \frac{C_{TES}}{G}\frac{1}{1-\mathscr{L}_I}$. For this simple model, the real part of the impedance plotted against the imaginary part gives a semi-circle. However, as seen in Fig. 4, impedance measurements of our gamma-ray microcalorimeters show clear deviation from a semi-circle and can not be fit using the simple one-body model, even when the devices have not yet had an absorber attached. For data on other samples, not shown, the two separate poles can be even more clearly distinguished.

The additional poles seen in our devices are most easily explained by adding an extra body, thus adding another coupled differential equation. This additional

CP1185, *Low Temperature Detectors LTD 13, Proceedings of the 13th International Workshop*
edited by B. Cabrera, A. Miller, and B. Young
2009 American Institute of Physics 978-0-7354-0751-0/09/$25.00

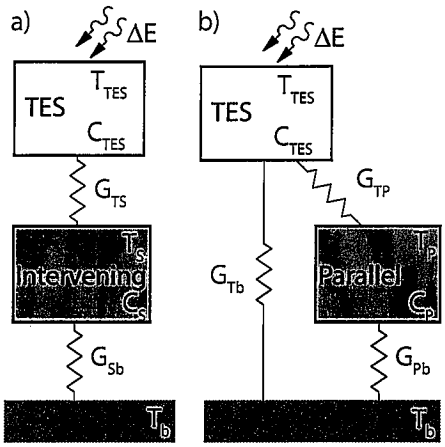

FIGURE 1. The possible two-body thermal models for TES; a) an intervening heat capacity and b) a parallel heat capacity. The dangling heat capacity model is equivalent to the parallel heat capacity without G_{Pb} shown in red.

body can be added between the TES and the heat bath as an intervening heat capacity (Fig. 1a) or as a dangling body off of the TES (Fig. 1b). The dangling heat capacity model is equivalent to one of the models we use for our devices with attached absorbers except when modeling the absorber we use larger heat capacities and thermal conductances. An interesting extension of the dangling body adds a thermal conductance between the dangling body and the heat bath, forming a parallel path for heat transfer (shown in red).

A potential candidate for the extra body is the SiN membrane supporting the TES. Recent measurements above 300 mK by the Withington group at Cambridge [8] suggest that at low temperatures the heat capacity of SiN is on the order of 10^3 times larger then one would expect from naive calculations using the Debeye model and this extra heat capacity scales linearly with temperature. Extrapolating their data to the $T_c = 124$ mK of our devices gives a heat capacity of 2 pW/K which is similar to that of our TESs. We speculate that the heat capacity of the SiN could be the other body suggested by our impedance data. However, the choice of two-body model is presently ambiguous. In this paper we compare possible models in a parameter range consistent with the calculated SiN heat capacity.

The impedance of these two-body models can be calculated as extensions of the formalism that describe the simple microcalorimeter. Power flow between heat capacities C_A and C_B at temperature T_A and T_B respectively is given by

$$P_{AB} = k_{AB}(T_A^n - T_B^n). \tag{3}$$

where n is the exponent of power flow and the prefactor k can be calculated from the thermal conductance (G_{AB}), which is defined as $\delta P/\delta T$ giving

$$G_{AB}(T_A) = nk_{AB}T_A^{n-1}, \tag{4}$$

We refer to a thermal conductance between bodies A and B referenced at the temperature of a body A as $G_{AB(A)}$. We will assume that the value of n is the same for all thermal conductances, which is reasonable for models describing SiN, but clearly not sufficient for models where the dangling heat capacity describes an attached absorber.

The intervening heat capacity will have a equilibrium temperature (T_{S0}) somewhere between that of the equilibrium temperature of the TES (T_c) and the bath (T_b). The equilibrium temperature of the intervening heat capacity can be calculated assuming power balance in each of the bodies, giving

$$T_{S0}^n = \frac{1}{k_{TS}+k_{Sb}}\left(k_{TS}T_c^n + k_{Sb}T_b^n\right). \tag{5}$$

The equilibrium temperature for the parallel heat capacity (T_{P0}) is calculated in the same way giving

$$T_{P0}^n = \frac{1}{k_{TP}+k_{Pb}}\left(k_{TP}T_c^n + k_{Pb}T_b^n\right). \tag{6}$$

When comparing the different models, we require that the total power flow and hence the effective overall conductance (G) be the same and fixed to the value extracted from the I-V curves. Given ratios of the k values for each thermal conductance obtained from geometric arguments, the individual k values and Gs are calculated such that the overall power flow to the heat bath is same for all models.

To calculate the impedance of the two body models, the differential equations are modified by adding a third coupled differential equation for the new body and modifying the relevant terms that describe the heat flow. For the case of the intervening heat capacity the resulting impedance is given by

$$Z_T(\omega) = R_0(1+\beta_I) + \frac{G_{etf}R_0(2+\beta_I)}{\left(-G_{etf}+G_{TS(T)}+i\omega C_{TES}\right)-\frac{G_{TS(T)}G_{TS(S)}}{\left(G_{TS(S)}+G_{Sb}+i\omega C_S\right)}}, \tag{7}$$

where C_S is the heat capacity of the intervening body (S) and G_{TS} and G_{Sb} are the thermal conductance between S and the TES and heat bath respectively. For convenience we have defined an effective thermal conductance from the electrothermal feedback as $G_{etf} = P_{J0}\alpha_I/T_0$. For the parallel case the resulting impedance is

$$Z_T(\omega) = R_0(1+\beta_I) + \frac{G_{etf}R_0(2+\beta_I)}{\left(-G_{etf}+G_{Tb}+G_{TP(T)}+i\omega C_{TES}\right)-\frac{G_{TP(T)}G_{TP(P)}}{G_{TP(P)}+G_{Pb}+i\omega C_P}} \tag{8}$$

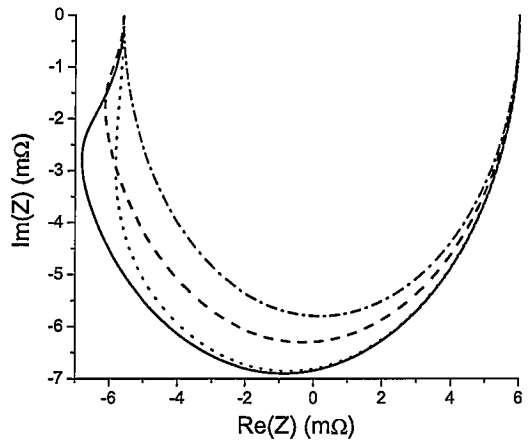

FIGURE 2. Im(Z) versus Re(Z) for the simple TES (black dash-dotted line), the intervening heat capacity (green dotted line), dangling heat capacity (red solid line) and parallel heat capacity (blue dashed line).

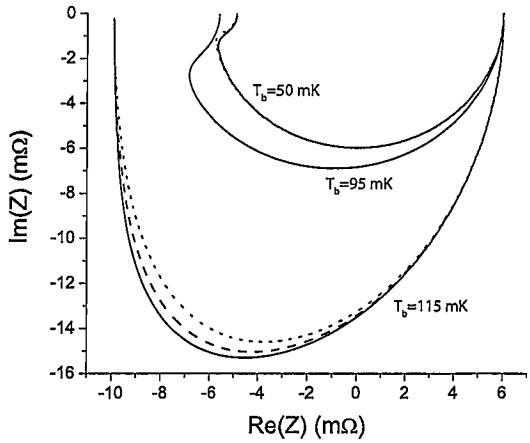

FIGURE 3. Comparison of the two-body models, dangling (red solid lines), parallel (blue dashed line) and intervening body model (green dotted lines) at three different bath temperatures, 115 mK, 95 mK, and 50 mK. At 95 mK, all three lines are made to overlap and are shown as a solid black line.

where C_P is the heat capacity of the parallel body (P) and G_{TP} is the thermal conductance from the TES to body P, G_{Pb} is the thermal conductance from body P to the bath, and G_{Tb} is the thermal conductance between the TES and body P.

Figure 2 shows the different models for parameters consistent with our devices: $T_c = 124$ mK, $T_b = 95$ mK, $n = 3.1$, $R_0 = 4$ mΩ, $\alpha_I = 40$, $\beta_I = 0.5$, $C_{TES} = 3$ pJ/K and $G(T_c) = 0.5$ nW/K. The k values are chosen to be the same except in the parallel case where $0.5k_{Pb} = k_{TP} = k_{Tb}$. Since we required the total power flowing to the bath be the same, all models have the same impedance at low frequencies where they are only functions of the R_0, β_I, G_{etf} and the total thermal conductance G that we required to be the same for all models. At high frequencies, the temperatures of the bodies cannot react to the rapidly changing bias current and the TES has an impedance $Z = R_0(1+\beta_I)$. At intermediate frequencies all two body models add an extra pole to the impedance at a frequency that is strongly dependent on the magnitude of the heat capacity of the second body relative to the heat capacity of the TES and the ratios of the thermal conductances.

Equation 7 and Eq. 8 have the same behavior as a function of frequency and therefore can all give the same shape. Comparing the intervening and dangling model, there is always a heat capacity ($C_s > C_p$) where the models have the same impedance as a function of frequency. Assuming predicted values for our devices, the heat capacity of an intervening body needs to be a few times larger to achieve a similar behavior. In other words, for the same heat capacity and a set ratio of k values the dangling heat capacity gives a larger deviation from the simple TES model than an intervening heat capacity. A similar comparison can be made for the the dangling and parallel models, where for a given G_{Pb}, the impedances can can be made the same if one increases the heat capacity of C_P and increases G_{TP}. For the previous parameters and $k_{Tb} = 0.2k_{Pb}$, to get the same impedance we must scale k_{TP} so that $k_{Tb} = 1.35k_{TP}$ and make C_P three times larger.

The models are more distinguishable as functions of bath temperature, since the the temperature of the dangling heat capacity stays fixed at T_c while the temperature of the heat capacity in the intervening and parallel models get pulled to lower temperatures by the bath. The heat capacity and associated G values of the intervening body and parallel body models must scale with temperature while those of the dangling body remain fixed. Figure 3 compares the various models at 115, 95 and 50 mK. At 95 mK, the parameters have been scaled so that all two-body models overlap as explained in the previous paragraph. At the different temperatures, the parameters C_S, C_P, G_{TS}, G_{Sb}, G_{TP} and G_{Pb} have been scaled for the bath temperature, linearly for C_S and C_P [8] and with a $n = 3.1$ for all G's. The plot shows that, with enough free parameters the models can be indistinguishable at one temperature but then are distinguishable when data taken at different Tb are analyzed together.

IMPEDANCE MEASUREMENTS

We have measured TES devices designed for gamma spectroscopy at energies around 100 keV. The details of these devices along with spectra obtained with them have been reported previously [9]. However, it is worth

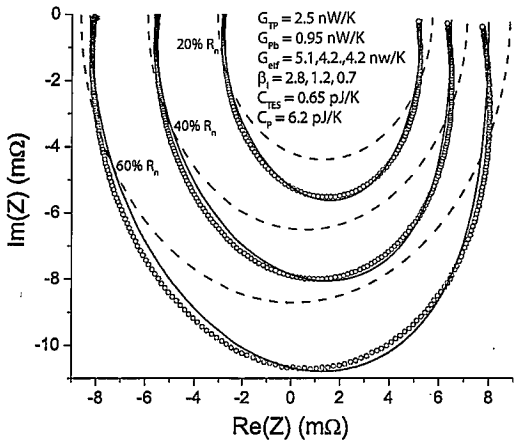

FIGURE 4. Global fits to impedance data (circles) for a simple one-body model (dashed lines) and the dangling two-body model (solid lines) at three different bias points 20% (black), 40% (red) and 60% (green) of the normal resistance. The best fit parameters for the dangling body model are given in the inset.

repeating that the SiN membrane is 1.4 x 1.4 mm^2 by 1 μm thick and that the T_c is 124 mK. In order to obtain initial information about the TES, the current-voltage characteristics of the TES are measured at different bath temperatures. These curves are used to obtain the Joule heating power at a given TES resistance as a function of the bath temperature. This data can then be fit with a power-law dependence to obtain information such as G, n, and T_c.

We obtained the transfer function by applying a sine wave with an amplitude small enough to stay in the small signal limit of our TES model. The sine wave is summed with the bias voltage and the frequency response is obtained by stepping the frequency over the range desired. The measurement is performed using a dynamic signal analyzer that sweeps the frequency of the applied signal and measures the response from the NIST SQUID feedback electronics. This method allows data with excellent signal to noise to be taken in a relatively short period of time. Each sweep was on the order of 8 minutes. The speed of the measurement allows many different devices to be measured at multiple bias points and temperatures in a single ADR cycle. The data obtained by the dynamic signal analyzer contains the response of the overall circuit. The impedance of the bias resistors, coupling inductors and other circuit parasitics are included in the raw data. However, the TES response is independent of frequency when it is biased in the superconducting and normal states. We can use this information to remove the effect of the remainder of the measurement circuit and obtain the response of the TES alone [5].

Figure 4 shows measured impedance data at 3 different bias points. The dashed lines are global fits using the simple model at the corresponding bias point, while the fine solid lines are fits using a two body model with a dangling heat capacity for the parameters in the inset. While the two body fits do not match the data perfectly they do show considerable agreement considering the three bias points share all parameters except for the resistance, α_I and β_I. We are currently in the process of fitting the data using the parallel heat capacity model.

ACKNOWLEDGMENTS

We gratefully acknowledge the support of the U.S. Department of Energy through the Office of Nonproliferation Research and Development.

REFERENCES

1. M. Lindeman, S. Bandler, R. Brekosky, J. Chervenak, E. Figueroa-Feliciano, F. Finkbeiner, M. Li, and C. Kilbourne, *REVIEW OF SCIENTIFIC INSTRUMENTS* **75**, 1283–1289 (2004), ISSN 0034-6748.
2. M. Galeazzi, and D. McCammon, *JOURNAL OF APPLIED PHYSICS* **93**, 4856–4869 (2003), ISSN 0021-8979.
3. J. Vaillancourt, *REVIEW OF SCIENTIFIC INSTRUMENTS* **76** (2005), ISSN 0034-6748.
4. T. Saab, S. Bandler, J. Chervenak, E. Figueroa-Feliciano, F. Finkbeiner, N. Iyomoto, R. Kelley, C. Kilbourne, M. Lindeman, F. Porter, and J. Sadleir, *NUCLEAR INSTRUMENTS & METHODS IN PHYSICS RESEARCH SECTION A* **559**, 712–714 (2006), ISSN 0168-9002.
5. M. A. Lindeman, K. A. Barger, D. E. Brandl, S. G. Crowder, L. Rocks, and D. McCammon, *REVIEW OF SCIENTIFIC INSTRUMENTS* **78** (2007), ISSN 0034-6748.
6. B. L. Zink, J. N. Ullom, J. A. Beall, K. D. Irwin, W. B. Doriese, W. D. Duncan, L. Ferreira, G. C. Hilton, R. D. Horansky, C. D. Reintsema, and L. R. Vale, *APPLIED PHYSICS LETTERS* **89** (2006), ISSN 0003-6951.
7. K. Irwin, and G. Hilton, "Transition-edge sensors," in *CRYOGENIC PARTICLE DETECTION*, 2005, vol. 99 of *TOPICS IN APPLIED PHYSICS*, pp. 63–149.
8. K. Rostem, D. Glowacka, D. Goldie, and S. Withington, "Thermal conductance measurements for the development of ultra low-noise transition-edge sensors with a new method for measuring the noise equivalent power," in *Proceedings of the SPIE*, 2008, vol. 7020, p. 70200L (11 pp.), ISSN 0277-786X.
9. N. Jethava, J. N. Ullom, D. A. Bennett, W. B. Doriese, J. A. Beall, G. C. Hilton, R. D. Horansky, K. D. Irwin, E. Sassi, L. R. Vale, M. K. Bacrania, A. S. Hoover, P. J. Karpius, M. W. Rabin, C. R. Rudy, and D. T. Vo, *Applied Superconductivity, IEEE Transactions on* **PP**, 530–533 (2009), ISSN 1051-8223.